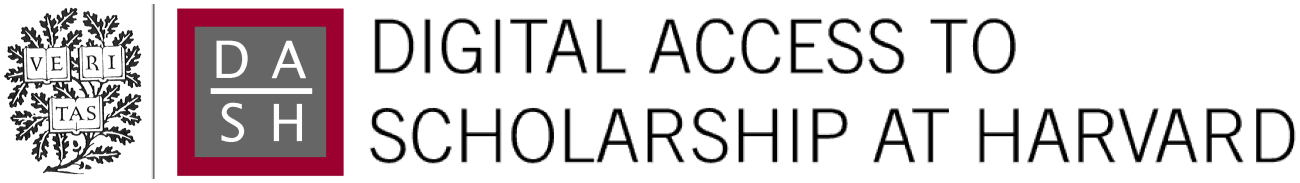

Modeling of cardiac muscle thin films: Pre-stretch, passive and active behavior

Supporting Material for Modeling of Cardiac Muscular Thin Films: Pre-stretch, Passive and Active Behavior

Jongmin Shim[1], Anna Grosberg[2], Janna C. Nawroth[3], Kevin Kit Parker[2], and Katia Bertoldi[1]

[1]*School of Engineering and Applied Science, Harvard University, Cambridge, MA*
[2]*Disease Biophysics Group, Wyss Institute for Biologically Inspired Engineering, School of Engineering and Applied Science, Harvard University, Cambridge, MA*
[3]*Division of Biology, California Institute of Technology, Pasadena, CA*

S1 Experimental Methods

This section provides a detailed description of the preparation of the silicone thin film and cell harvesting procedure.

S1.1 Manufacturing the Silicone Thin Films

The silicone thin films were prepared via a multi-step spin coating process, extending a previously published method (Feinberg et al., 2007) in order to allow for higher experimental throughput. The samples prepared this way have been dubbed "Heart on a chip". To prepare the chips, a section of glass ($7.5cm \times 11cm$) was sonicated and covered with a protective film (Static Cling Film, McMaster-Carr, Robbinsville, NJ) on both sides. Rectangles ($1cm \times 0.6cm$) were cut out of the top protective film, and poly(N-isopropylacrylamide) (PIPAAm, Polysciences, Inc., Warrington, PA) in 1-butanol (10% w/v) was spin-coated onto the uncovered portions of the glass, and then the top protective film was removed. The silicone polymer polydimethylsiloxane (PDMS, Sylgard 184-Dow Corning, Midland, MI) was pre-cured for 1 to 6 hours, spin coated onto the glass, and cured for 8 hours at $65°C$. The bottom protective film was removed, and the glass section was cut into cover slips of $1.4cm \times 1.2cm$. From each glass section, two cover slips were used to measure the thickness of the PDMS layer using a profilometer (Dektak 6M, Veeco Instruments Inc., Plainview, NY). The PDMS surface of the cover slip was functionalized and sterilized for 8 minutes in UV ozone (Model No. 342, Jetlight Company, Inc., Phoenix, AZ). Fibronectin (FN, Sigma, St. Louis, MO or BD Biosciences, Sparks, MD) was micropatterned onto the surface via microcontact printing with a brick pattered PDMS stamp (each brick was $20\mu m$ wide and $100\mu m$ long, and each short edge terminated with $5\mu m$ long saw-tooth, Bray et al., 2008), such that the brick pattern would be perpendicular or at some tilted angle to the long edge of the cover slip. The gaps in the pattern were blocked by incubating the cover slip in Pluronics F127 (BASF Group, Parsippany, NJ) for 5 minutes, and then the chips were stored at $4°C$ until cell seeding. Three different PDMS thickness were made though this procedure: $14.5\mu m$, $18.0\mu m$, $23.0\mu m$.

S1.2 Cell harvesting, Seeding, and Culture

Cell harvesting was conducted in accordance with the guidelines of Institutional Animal Care and Use Committee of Harvard University. Cardiomyocytes were harvested and isolated based on published protocols (Adams et al., 2007). Briefly, ventricles were extracted from two-day-old neonatal Sprague-Dawley rats (Charles River Laboratories, Wilmington, MA) and homogenized by washing in Hanks balanced salt solution, then incubated with trypsin overnight at $4°C$. To release the myocytes into solution, the ventricular tissue was digested with collagenase at $37°C$. Cells were re-suspended in M199 culture medium supplemented with 10% (v/v) heat-inactivated fetal bovine serum (FBS), $10mM$ HEPES, $3.5g/L$ glucose, $2mM$ L-glutamine, $2mg/L$ vitamin B-12, and $50U/ml$ penicillin. The myocytes were seeded on the substrates at a density of 400,000 cells per cover slip (round, diameter of $18mm$), and cultured for a period of four days prior to running the assay. During the initial 48 hours, the cells were kept at $37°C$ and $5\%CO_2$ with 10% FBS media in the culture; thereafter, the maintenance media (2% FBS) was used. The measured cell thickness was approximately $4.0\mu m$.

S1.3 Contractility Experiments

To run the contractility experiments, the chip was moved to a Petri dish with $37°C$ normal Tyrode's solution ($1.192g$ of HEPES, $0.901g$ of glucose, $0.265g$ of $CaCl_2$, $0.203g$ of $MgCl_2$, $0.403g$ of KCl, $7.889g$ of $NaCl$, and $0.040g$ of NaH_2PO_4 per liter of deionized water; reagents from Sigma, St. Louis, MO). The PDMS elastic layer was cut such as to leave the PDMS along the border of the cover slip intact, while in the center there were two rows of three to four rectangles (approximately $2mm \times 3.5mm$) separated by approximately $1mm$, and connected to the PDMS border by one edge (see Figs. **??**). The unwanted film was peeled away, exposing the temperature-sensitive PIPAAm beneath the rectangular strips and causing it to dissolve as the solution was allowed to cool down towards room temperature. Subsequently, the rectangular films were free to move vertically up from the plane of the cell culture, without completely separating from the chip. The chip with six or eight rectangular films was moved to a heated bath ($34°C - 37°C$) under a stereomicroscope (Model MZ6 with darkfield base, Leica Microsystems, Inc., Wetzlar, Germany), and the dynamics of the films was recorded from above at 120 $frames/sec$ (Basler A602f camera, Exton, PA). Several snapshots from the recorded movies are shown in Figs. **??** and **??**.

While the film laid flat on the glass, both its length and width were measured. As the films contracted away from the surface, the horizontal projection was recorded. Unimpeded films would first isometrically deform to a curvature corresponding to the diastolic tension in the cells, and then continue to deform until peak systole. For substrates with cells aligned with the length of the film, the observed deformation was a shortening of the projection, described in Fig. **??** (top). On the other hand, the substrates with cells at an angle to the length of the film showed the inclined free edge of the film (see Fig. **??** (bottom)), so an appropriate projection length needed to be defined in order to obtain the curvature of the MTFs. To ensure all films on the chip were moving at once, the myocytes were field-stimulated at $1.5Hz$ with 5 to $20V$ using an external field stimulator (Myopacer, IonOptix Corp., Milton, MA) which applied a $10msec$ square wave pulse.

S2 Constitutive Modeling of Bio-hybrid Films

In this section, we first summarize the equations governing the nonlinear deformation of hyperelastic materials, following the formulation previously introduced by **?**. Then, the equations are specialized to capture the behavior of the elastomeric substrate and the cardiac myocytes.

As mentioned in Section 1, cardiac myocytes comprise highly aligned myofibrils, so their behavior is captured extending the formulation previously developed to model fiber reinforced elastomers (e.g., Spencer, 1984).

S2.1 General Formulation

Let $\mathbf{F} = \partial\mathbf{x}/\partial\mathbf{X}$ be the deformation gradient mapping a material point from the reference position $\mathbf{X}$ to its current position $\mathbf{x}$, and $J = \det\mathbf{F}$ be its determinant. The behavior of nearly incompressible materials is effectively described by splitting the deformation locally into volumetric (denoted by superscript v) and isochoric (denoted by superscript i) components as

$$\mathbf{F} = \mathbf{F}^v \cdot \mathbf{F}^i, \quad \text{where} \quad \mathbf{F}^v = J^{1/3}\mathbf{1}, \quad \mathbf{F}^i = J^{-1/3}\mathbf{F}. \tag{S1}$$

For an isotropic hyperelastic material, the strain energy density ψ is a function of the three invariants of $\mathbf{C} = \mathbf{F}^T \cdot \mathbf{F}$, $\psi = \psi(I_1, I_2, I_3)$. Based on the kinematic assumption (S1), a decoupled form for ψ is introduced

$$\psi = \psi^v(J) + \psi^i(\bar{I}_1, \bar{I}_2), \tag{S2}$$

with

$$\bar{I}_1 = \mathrm{tr}\mathbf{C}^i, \quad \bar{I}_2 = \frac{1}{2}\left[\left(\mathrm{tr}\mathbf{C}^i\right)^2 - \mathrm{tr}\left(\mathbf{C}^{i^2}\right)\right]. \tag{S3}$$

When an isotropic material is reinforced by a family of fibers with direction $\mathbf{a}_0$ in the reference configuration, the isochoric part of the strain energy can be expressed as a function of not only $\bar{I}_1$ and $\bar{I}_2$, but also two additional invariants $(\bar{I}_4, \bar{I}_5)$ depending on $\mathbf{a}_0$ (Spencer, 1984),

$$\psi^i = \psi^i(\bar{I}_1, \bar{I}_2, \bar{I}_4, \bar{I}_5), \tag{S4}$$

with

$$\bar{I}_4 = \mathbf{a}_0 \cdot \mathbf{C}^i \cdot \mathbf{a}_0 = \bar{\lambda}^2, \quad \bar{I}_5 = \mathbf{a}_0 \cdot \mathbf{C}^{i^2} \cdot \mathbf{a}_0. \tag{S5}$$

However, the dependence of the material response on $\bar{I}_2$ or $\bar{I}_5$ is generally weak, so that the isochoric part of the strain energy can be simplified as

$$\psi^i = \psi^i_{iso}\left(\bar{I}_1\right) + \psi^i_{ani}\left(\bar{I}_4\right), \tag{S6}$$

where ψ^i has been further decoupled into an isotropic, ψ^i_{iso}, and anisotropic, ψ^i_{ani}, contributions.

Finally, the Cauchy stress $\mathbf{T}$ is found by differentiating ψ with respect to $\mathbf{C}$ as

$$\mathbf{T} = \frac{2}{J}\mathbf{F}\frac{\partial \psi}{\partial \mathbf{C}}\mathbf{F}^T = \frac{\partial \psi^v}{\partial J}\mathbf{1} + \frac{2}{J}\left[\frac{\partial \psi^i_{iso}\left(\bar{I}_1\right)}{\partial \bar{I}_1}\mathrm{dev}\left(\mathbf{B}^i\right) + \bar{I}_4\frac{\partial \psi^i_{ani}\left(\bar{I}_4\right)}{\partial \bar{I}_4}\mathrm{dev}\left(\bar{\mathbf{a}} \otimes \bar{\mathbf{a}}\right)\right], \tag{S7}$$

where "dev" stands for deviatoric part of 2^{nd} order tensors, $\mathbf{B}^i = \mathbf{F}^i \cdot \mathbf{F}^{i^T}$ is the left Cauchy-Green tensor, and $\bar{\mathbf{a}} = \mathbf{F}^i \cdot \mathbf{a}_0 / \sqrt{\bar{I}_4}$ is the unit directional vector of fiber in the deformed configuration.

In the following two sections, the above general formulation is specialized to capture the behavior of the elastomeric substrate and the cardiac myocytes.

S2.2 Elastomeric Substrate Behavior

The elastomeric substrate is fabricated using PDMS, and its behavior is well captured using a neo-Hookean model, so that the strain energy density is given by

$$\psi = \psi^v\left(J\right) + \psi^i\left(\bar{I}_1\right) = \frac{\tilde{\kappa}}{2}\left(J-1\right)^2 + \frac{\tilde{E}}{6}\left(\bar{I}_1 - 3\right), \tag{S8}$$

where $\tilde{\kappa}$ and $\tilde{E}$ denote the bulk modulus and the initial elastic modulus of the elastomer, respectively.

Based on (S7), the Cauchy stress is given by:

$$\mathbf{T} = \tilde{\kappa}(J-1)\mathbf{1} + \frac{\tilde{E}}{3J}\mathrm{dev}\left(\mathbf{B}^i\right). \tag{S9}$$

S2.3 Cardiac Muscle Cell Behavior

The characteristic energy dissipative process of the cardiomyocite active contribution can be modeled by the physiological approach, which considers its true mechanism due to the actin potential under calcium flux (*e.g.*, Sainte-Marie et al., 2006; Chapelle et al., 2010). However, this approach is mathematically complex, and model parameter identification is challenging. In this article, instead, we take a simple, but effective phenomenological approach, where the active behavior is assumed to be elastic. While recently Böl et al. (2009) developed a phenomenological model of cardiac muscle cells, their model neglects the important effect of the pre-stretch that the muscle cells develop as they mature. This paper presents a 3-D phenomenological model that captures the two major features of cardiac muscles: the passive behavior inducing pre-stretched deformation and their active behavior including systole and diastole.

S2.3.1 Kinematics including Pre-stretch

Even when resting, muscle cells *in vivo* experience a state of stress due to their pre-stretched conditions. This can be clearly observed from the experimental data reported in Figs. **??** and Fig. **??**, showing a non-negligible MTF curvature during diastole. In order to account for such pre-stretched conditions, previous constitutive models introduced an *ad hoc* strain-shift in the stress-strain curve (Blemker et al., 2005; Böl and Reese, 2008; Calvo et al. (2010)). However, this strain-shift leads to a stress-strain curve that depends on the level of pre-stretch. In this paper, a different approach is adopted; inspired by the multiplicative decomposition introduced by Kroner-Lee (Kroner, 1960; Lee, 1969), the isochoric deformation gradient $\mathbf{F}^i$ in (S1) is decomposed into load-induced, $\mathbf{F}^{iL}$, and pre-stretched, $\mathbf{F}^{iS}$, contributions

$$\mathbf{F}^i = \mathbf{F}^{iL} \cdot \mathbf{F}^{iS}. \tag{S10}$$

Here, for the sake of simplicity, the pre-stretch is assumed to be fully developed during cell differentiation and maturation prior to the experiment, and not to be affected by the cell active response. If we also assume that the pre-stretch deformation is incompressible and the cells deform affinely, the pre-stretched contribution to the deformation gradient $\mathbf{F}^{iS}$ is given by

$$\mathbf{F}^{iS} = \mathbf{Q}\mathbf{\Lambda}\mathbf{Q}^T, \tag{S11}$$

where

$$\mathbf{\Lambda} = \hat{\lambda}_S \, \mathbf{e}_1 \otimes \mathbf{e}_1 + \left(\hat{\lambda}_S\right)^{-\frac{1}{2}} (\mathbf{e}_2 \otimes \mathbf{e}_2 + \mathbf{e}_3 \otimes \mathbf{e}_3) \tag{S12}$$

$$\mathbf{Q} = \cos\hat{\theta}\,(\mathbf{e}_1 \otimes \mathbf{e}_1 + \mathbf{e}_2 \otimes \mathbf{e}_2) + \sin\hat{\theta}\,(-\mathbf{e}_1 \otimes \mathbf{e}_2 + \mathbf{e}_2 \otimes \mathbf{e}_1) + \mathbf{e}_3 \otimes \mathbf{e}_3 \tag{S13}$$

where $\hat{\lambda}_S$ is the pre-stretch induced into the cardiac myocytes lying in the x_1-x_2 plane during maturation (*i.e.*, myogenesis and tissue development) and $\hat{\theta}$ is the angle identifying the cell alignment in the undeformed configuration (see Fig. **??**). The diastole curvatures of the experimental data reported in Figs. **??** and Fig. **??** clearly show a deviation in the pre-stretched response of the cells as a result of the diversity in cell conditions. Therefore, we expect the parameter $\hat{\lambda}_S$ *not to be uniquely determined*, but to be influenced by experimental factors such as ambient temperature/humidity, and age/health of the cells.

S2.3.2 Constitutive Equations for Passive and Active Behavior

In order to describe both passive (representing resting status) and active (including systole and diastole) behavior of cardiomyocytes, we specify their free energy as

$$\psi = \psi^v\left(J\right) + \psi^i_{iso}\left(\bar{I}_1\right) + \psi^{ip}_{ani}\left(\bar{I}_4\right) + \psi^{ia}_{ani}\left(\bar{I}_4, q\right), \tag{S14}$$

where q is the activation level of cardiac muscle cells. In the present model, while ψ^v and ψ^i_{iso} reflects the isotropic contribution of the intercellular part, ψ^{ip}_{ani} and ψ^{ia}_{ani} represent the passive and the active contributions of anisotropic effect of the myofibril, repectively.

Here, as for the elastomeric substrate, the volumetric free energy term is chosen as

$$\psi^v(J) = \frac{\hat{\kappa}}{2}\left(J-1\right)^2, \tag{S15}$$

and the isotropic contribution of the intercellular part is captured using a neo-Hookean formulation

$$\psi^i_{iso} = \frac{\hat{E}_c}{6}\left(\bar{I}_1 - 3\right), \tag{S16}$$

where $\hat{\kappa}$ denotes the bulk modulus of the cells and $\hat{E}_c$ is the initial elastic modulus of intercellular part. Several experimental studies (e.g., Le Guennec et al., 1990; Granzier and Irving, 1995; Palmer et al., 1996; Cazorla et al., 2000; Weiwad et al., 2000; Boron and Boulpaep, 2009) reveal that the passive response of cardiac cells is characterized by an exponential relation between stress and deformation (see Fig. **??**). In order to capture such behavior of cardiac cells, we propose the following free energy

$$\psi^{ip}_{ani}\left(\bar{\lambda}\right) = \frac{\hat{E}_p}{\hat{\alpha}^2}\left[e^{\hat{\alpha}(\bar{\lambda}-1)} - \hat{\alpha}(\bar{\lambda}-1) - 1\right], \tag{S17}$$

where $\bar{\lambda} = \sqrt{\bar{I}_4}$, $\hat{E}_p$ is the initial elastic modulus, and $\hat{\alpha}$ characterizes the monotonically increasing slope of the stress-strain relation of the passive response of the fibers. For the active response (see Fig. **??**), a bell-type relation between stress and deformation has been shown by several studies (e.g., Zajac, 1989; Weiwad et al., 2000; Boron and Boulpaep, 2009). Here, we simplify the active stress-stretch relation into a quadratic form, which is captured introducing the following free energy

$$\psi^{ia}_{ani}\left(\bar{\lambda}, q\right) = \begin{cases} \frac{\hat{P}q}{2(1-\hat{\lambda}_o)^2}\left[2(1-2\hat{\lambda}_o)\ln\bar{\lambda} + (4\hat{\lambda}_o - \bar{\lambda} - 1)(\bar{\lambda}-1)\right], & \text{if } 1 < \bar{\lambda} < (2\hat{\lambda}_o - 1) \\ 0, & \text{otherwise} \end{cases} \tag{S18}$$

where $\hat{P}$ is the isometric twitch stress (*i.e.*, the maximum contraction force per unit cross-sectional area) and $\hat{\lambda}_o$ is the optimal stretch (*i.e.*, the stretch at which the maximum active stress is attained). Since Fig. **??** and Fig. **??** clearly show that diversity in cell conditions causes large variations of the peak amplitudes, as the pre-stretch $\hat{\lambda}_S$, the parameter $\hat{P}$ is also treated as a *non-uniquely determined* property of cultured cardiac tissue. Finally, the activation level q is a function of time and is defined as

$$q(t) = \left(\frac{t}{\hat{T}}\right)^2 \exp\left[1 - \left(\frac{t}{\hat{T}}\right)^2\right], \tag{S19}$$

where $\hat{T}$ is the characteristic contraction time.

Based on (S7), the proposed free energy results in the following Cauchy stress

$$\mathbf{T} = \mathbf{T}^v + \mathbf{T}^i_{iso} + \mathbf{T}^{ip}_{ani} + \mathbf{T}^{ia}_{ani}, \tag{S20}$$

where

$$\mathbf{T}^v = \hat{\kappa}(J-1)\mathbf{1} \tag{S21}$$

$$\mathbf{T}^i_{iso} = \frac{\hat{E}_c}{3J}\mathrm{dev}\left(\mathbf{B}^i\right) \tag{S22}$$

$$\mathbf{T}^{ip}_{ani} = \frac{\hat{E}_p\bar{\lambda}}{\hat{\alpha}J}\left[e^{\hat{\alpha}(\bar{\lambda}-1)}-1\right]\mathrm{dev}(\bar{\mathbf{a}}\otimes\bar{\mathbf{a}}), \tag{S23}$$

$$\mathbf{T}^{ia}_{ani} = \begin{cases} \frac{\hat{P}q}{J}\left[1-\left(\frac{\bar{\lambda}-\hat{\lambda}_o}{1-\hat{\lambda}_o}\right)^2\right]\mathrm{dev}(\bar{\mathbf{a}}\otimes\bar{\mathbf{a}}), & \text{if } 1<\bar{\lambda}<(2\hat{\lambda}_o-1) \\ 0, & \text{otherwise} \end{cases} \tag{S24}$$

S3 Parameter Identification for the Constitutive Model

This section presents the procedure to identify the 11 material parameters entering into the proposed 3-D constitutive model. While the material parameters for the elastomeric substrate are provided by the manufacturers, the parameters needed for the cardiac muscle cells are obtained from both literature and contraction assays performed with neonatal rat ventricular myocytes micropatterned on PDMS thin films.

S3.1 Summary of Model Parameters

The proposed constitutive model requires 11 material constants

- Elastomeric substrate
  - $\tilde{E}$ Initial elastic modulus
  - $\tilde{\kappa}$ Initial bulk modulus
- Pre-stretched deformation of cardiac muscle cells
  - $\hat{\theta}$ Angle defining the initial alignment of the cells within the $x_1 - x_2$ plane
  - $\hat{\lambda}_S$ Pre-stretch developed in the cardiomyocytes during cell maturation
- Volumetric and isotropic behavior of cardiac muscle cells
  - $\hat{E}_c$ Initial elastic modulus of intercellular part
  - $\hat{\kappa}$ Initial bulk modulus
- Passive fiber behavior of cardiac muscle cells
  - $\hat{E}_p$ Initial elastic modulus of fiber
  - $\hat{\alpha}$ Constant related to the slope of stress-strain relation of passive fiber
- Active fiber behavior of cardiac muscle cells
  - $\hat{P}$ Isometric twitch stress
  - $\hat{\lambda}_o$ Optimal stretch for the maximum active stress
  - $\hat{T}$ Characteristic time scale for contraction

S3.2 Elastomeric Substrate ($\tilde{E}$, $\tilde{\kappa}$)

Only two material constants ($\tilde{E}$, $\tilde{\kappa}$) are required to model the elastomeric substrates. The initial elastic modulus is directly specified by the manufacturer as $\tilde{E} = 1.5$ MPa, while its incompressible behavior ($\tilde{\nu} = 0.49$) yields an initial bulk modulus $\tilde{\kappa} = 25$ MPa.

S3.3 Cardiac Myocytes

The proposed model requires seven material-specific parameters ($\hat{\kappa}$, $\hat{E}_c$, $\hat{E}_p$, $\hat{\alpha}$, $\hat{P}$, $\hat{\lambda}_o$, $\hat{T}$) and two geometric-specific parameters ($\hat{\theta}$, $\hat{\lambda}_S$). Most of model parameters are available in the literature. The paper by Weiwad et al. (2000) provides in a single article nearly all the required test results to identify the material paramors entering into the proposed material model. Moreover, all their data are in a good agreement with similar test results for the heart muscle of adult rats (*i.e.*, Granzier and Irving, 1995, Palmer et al., 1996 for passive behavior and Nishimura et al., 2000, Palmer et al., 1996 for active behavior). Thus, the test results presented in Weiwad et al. (2000) are used to identify five material-specific parameters entering into the proposed constitutive model.

Experiments with straight cell alignment (Section 2) are used to identify the remaining three parameters; two of which (*i.e.*, $\hat{P}$, $\hat{\lambda}_S$) are experimental-conditions-specific, and one of which (*i.e.*, $\hat{T}$) is the characteristic time scale of contractile behavior under the stimulating electric pulse. Here, we assume that the cell conditions affect only the twitch stress $\hat{P}$ and the pre-stretch $\hat{\lambda}_S$.

S3.3.1 Isochoric Behavior of Intercellular Part ($\hat{E}_c$) and Isochoric Passive Behavior of Fiber Part ($\hat{E}_p$, $\hat{\alpha}$)

Several researchers have reported experimentally measured values for Young's modulus of non-activated rat cardiac myocytes by using atomic force microscopy (e.g., Lieber et al., 2004) or custom-designed force transducer (e.g., Weiwad et al., 2000). The measured values varies from $20kPa$ to $45kPa$ depending on the experimental protocols and the ages of rats. Following Weiwad et al. (2000), we use a Young's modulus, $\hat{E}_{passive} = 23kPa$ (see Fig. **??**). From (S20), recall that the measured Young's modulus of the non-activated cell can be decomposed into the contribution of intercellular part and passive fiber part. Here, we assume that the passive fiber part is mainly responsible for the passive elastic behavior, so that $\hat{E}_p = 21kPa$ and $\hat{E}_c = 2.3kPa$. Note that the passive stress ($T_{11}^{passive}$) can be expressed as:

$$T_{11}^{passive} = \left(T_{iso}^{i}\right)_{11} + \left(T_{ani}^{ip}\right)_{11}, \tag{S25}$$

where using incompressibility each stress contribution can be determined from the reduced form of (S22) and (S23):

$$\left(T_{iso}^{i}\right)_{11} = \frac{\hat{E}_c}{3}\left(\bar{\lambda}^2 - \frac{1}{\bar{\lambda}}\right), \tag{S26}$$

$$\left(T_{ani}^{ip}\right)_{11} = \frac{\hat{E}_p \bar{\lambda}}{\hat{\alpha}}\left[e^{\hat{\alpha}(\bar{\lambda}-1)} - 1\right]. \tag{S27}$$

By curve-fitting the experimental results with the above equations (see Fig. **??**), we obtain $\hat{\alpha} = 5.5$.

S3.3.2 Isochoric Active Behavior of Fiber Part ($\hat{P}$, $\hat{\lambda}_o$, $\hat{T}$)

Weiwad et al. (2000) have reported the evaluation of the isometric twitch stress as a function of calcium concentration (see Fig. **??**). Note that a constant calcium concentrations of $pCa = 2.74$ was employed throughout the essay tests presented in Section 2. In order to get its overall dependence on the stretch, all the active tension-stretch relations are normalized by its maximum value, and then curve-fitted by the proposed quadratic form of active stress-stretch relation for uniaxial loading case:

$$\left(T^{ia}_{ani}\right)_{11} = \begin{cases} \hat{P}q\left[1 - \left(\frac{\bar{\lambda}-\hat{\lambda}_o}{1-\hat{\lambda}_o}\right)^2\right], & \text{if } \ 1 < \bar{\lambda} < (2\hat{\lambda}_o - 1) \\ 0, & \text{otherwise} \end{cases} \tag{S28}$$

As a result, we obtain $\hat{\lambda}_o = 1.24$, as shown in Fig. **??**. As described in Section 4, the range of the isometric twitch stress of $\hat{P} \in [2.8,\ 21.6]kPa$ is determined from experiments with straight cell alignment presented in Section 2. The characteristic contraction time can be determined by measuring the time when the signal reaches its maximum value after the activation starts. Fig. **??** shows a typical profile of the active amplitude history, and $\hat{T} = 0.21sec$ was determined.

S3.3.3 Volumetric Behavior ($\hat{\kappa}$)

For simplicity, we assume that the cardiac muscle is nearly incompressible and its volumetric behavior is determined by the passive response. Thus, using $\hat{E}_{passive} = 23kPa$ and $\hat{\nu} = 0.49$, we obtain a bulk modulus of $\hat{\kappa} = \frac{\hat{E}_{passive}}{3(1-2\nu)} = 380kPa$.

S3.3.4 Isochoric Pre-stretch Behavior ($\hat{\theta}$, $\hat{\lambda}_S$)

For the model parameter identification, the controlled test set (*i.e.*, the case with the straight cell alignment) with $\hat{\theta} = 0^\circ$ is used. It is known that the level of pre-stretch (or pre-stress/pre-load) developed during cell maturation depends on the properties of substrate.

From the assay experiments in Section 2, we obtain $\hat{\lambda}_S \in [1.11, 1.18]$. This range of values for pre-stretch have been also reported under similar experimental conditions using a silicon substrate (e.g., Mansour et al., 2004).

S4 Parametric Studies

In this Section, we explore the effect of important parameters within MTF such as the PDMS thickness, the isometric twitch stress of cells, the pre-stretch of cells, and the frequency of field-stimulation.

S4.1 Effect of PDMS Thickness

Here, the effect of PDMS thickness on the response of the MTF is explored by varying $\tilde{t}$ from $13.0\mu m$ to $28.0\mu m$. Meanwhile, the average value of the two cell-condition-dependent parameters are used (*i.e.*, $\hat{\lambda}_S = 1.14$ and $\hat{P} = 9.0kPa$), and all other model parameters are also unchanged throughout the simulations.

Fig. S1a shows the effect of PDMS thickness on the total curvature (K) of MTF. As expected, an increase in PDMS thickness leads to a decrease in curvature. To quantify this behavior, the

total curvature is decomposed into pre-stretch (K_p), and active (K_a), contributions, so that

$$K = K_p + K_a. \tag{S29}$$

Fig. S1b reports the evolution of maximum passive and active curvature contributions (*i.e.*, $max(K_p)$ and $max(K_a)$) as a function of the PDMS thickness. The pre-stretch contribution of the curvature can be also estimated by applying a recent modification of the Stoney's equation (*i.e.*, **?**). Assuming that the layer of cells is much thinner than that of substrate, the Stoney *curvature* equation predicts the curvature of the bilayer film as

$$K_{stoney} = \frac{6(\hat{E}_c + \hat{E}_p)\ \ln\hat{\lambda}_S}{\tilde{E}\tilde{t}} \left(\frac{\hat{t}}{\tilde{t}}\right) \left(1 + \frac{\hat{t}}{\tilde{t}}\right). \tag{S30}$$

The pre-stretch induced curvature predicted by (S30) is also reported in Fig. S1b, and a good agreement with the pre-stretch contribution from the FEM calculations is observed.

S4.2 Effect of Isometric Twitch Stress of Cells

We vary $\hat{P}$ from 0 to $30.0kPa$ while keeping all other parameters unchanged, including $\tilde{t} = 18.0\mu m$ and $\hat{\lambda}_S = 1.14$.

Fig. S1c shows the effect of isometric twitch stress on the curvature of MTFs. While the passive contribution of the curvature ($max(K_p)$) is unaffected by $\hat{P}$, the active contribution ($max(K_a)$) is observed to vary almost linearly with $\hat{P}$ (Fig. S1d).

S4.3 Effect of Cell Pre-stretch

The effect of pre-stretch on the cardiac muscle cell response is investigated by varying $\hat{\lambda}_S$ from 1.00 (*i.e.*, no pre-stretch) to 1.39 while keeping all other parameters unchanged and using $\tilde{t} = 18.0\mu m$ and $\hat{P} = 9.0kPa$.

Figure S1e reports the time history of film curvature for various level of cells pre-stretch. The results clearly show that the level of cell pre-stretch affects the curvature both during cell maturation and activation. Interestingly, for the active response, we observe the quadratic relation between the pre-stretch and the active curvature contribution. Thus, this study suggests that the maximum level of active response (*i.e.*, the maximum active mobility) for the MTFs can be achieved by introducing an optimal pre-stretch value. Moreover, Fig. S1f clearly show that the Stoney equation (S30) largely underestimates the MTF curvature for large pre-stretch.

References

W.J. Adams, T. Pong, N.A. Geisse, S.P. Sheehy, B. Diop-Frimpong, and K.K. Parker. Engineering design of a cardiac myocyte. *Journal of Computer-Aided Materials Design*, 14(1):19–29, 2007.

S.S. Blemker, Pinsky P.M., and S.L. Delp. A 3d model of muscle reveals the causes of nonuniform strains in the biceps brachii. *Journal of Biomechanics*, 38:657–665, 2005.

M. Böl and S. Reese. Micromechanical modelling of skeletal muscles based on the finite element method. *Computer Methods in Biomechanics and Biomedical Engineering*, 11:489–504, 2008.

M. Böl, S. Reese, K.K. Parker, and E. Kuhl. Computational modeling of muscular thin film for cardiac repair. *Computational Mechanics*, 43:535–544, 2009.

W.F. Boron and E.L. Boulpaep. *Medical Physiology.* Saunders, 2009.

M.A. Bray, S.P. Sheehy, and K.K. Parker. Sarcomere alignment is regulated by myocyte shape. *Cell Motility and the Cytoskeleton*, 65(8):641–651, 2008.

B. Calvo, A. Ramirez, A. Alonso, J. Grasa, F. Soteras, R. Osta, and M.J. Munoz. Passive nonlinear elastic behaviour of skeletal muscle: Experimental results and model formulation. *Journal of Biomechancis*, 43:318–325, 2010.

O. Cazorla, J.-Y. Le Guennec, and E. White. Lenght-tension relationships of sub-epicaridal and sub-endocardial single ventricular myocytes from rat and ferret hearts. *Journal of Molecular and Cellular Cardiology*, 32:735–744, 2000.

D. Chapelle, J.F. Gerbeau, J. Sainte-Marie, and I.E. Vignon-Clementel. A poroelastic model valid in large strains with applications to perfusion in cardiac modeling. *Computational Mechanics*, 46:91–101, 2010.

A.W. Feinberg, A. Feigel, S.S. Shevkoplyas, S. Sheehy, G.M. Whitesides, and K.K. Parker. Muscular thin films for building actuators and powering devices. *Science*, 317(5843):1366–1370, 2007.

H.L. Granzier and T.C. Irving. Passive tension in cardiac muscle: contribution of collagen, titin, microtubules, and intermediate filaments. *Biophysical Journal*, 68:1027–1044, 1995.

E. Kroner. Allgemeine kontinuums theorie der versetzungen und eigenspannungen. *Archive for Rational Mechanics and Analysis*, 4:273–334, 1960.

J.-Y. Le Guennec, N. Peineau, J.A. Argibay, K.G. Mongo, and D. Garnier. A new method of attachment of isolated mamalian ventricular myocytes for tension recording: Length dependence of passive and active tension. *Journal of Molecular and Cellular Cardiology*, 22: 1083–1093, 1990.

E.H. Lee. Elastic-plastic deformation at finite strains. *Journal of Applied Mechanics*, 36:1, 1969.

S.C. Lieber, N. Aubry, J. Pain, G. Diaz, S.J. Kim, and S.F. Vatner. Aging increases stiffness of cardiac myocytes measured by atomic force microscopy nanoindentation. *AJP-Heart and Circulatory Physiology*, 287:H645–H651, 2004.

H. Mansour, P.P. de Tombe, A.M. Samarel, and B. Russell. Restoration of resting sarcomere length after uniaxial static strain is regulated by protein kinase cϵ and focal adhesion kinase. *Circulation Research*, 94:642–649, 2004.

S. Nishimura, S. Yasuda, M. Katoh, K.P. Yamada, H. Yamashita, Y. Saeki, K. Sunagawa, R. Nagai, T. Hisada, and S. Sugiura. Single cell mechanics of rat cardiomyocytes under isometric, unloaded, and physiologically loaded conditions. *AJP-Heart and Circulatory Physiology*, 287: H196–H202, 2000.

R.E. Palmer, A.J. Brady, and K.P. Roos. Mechanical measurements from isolated cardiac myocytes using a pipette attachment system. *AJP-Cell Physiology*, 270:C697–C704, 1996.

J. Sainte-Marie, D. Chapelle, R. Cimrman, and M. Sorine. Modeling and estimation of the cardiac electromechanical activity. *Computers and Structures*, 84:1743–1759, 2006.

A.J.M. Spencer. *Continuum Theory of the Mechanics of Fibre-reinforced Composites*. Springer-Verlag, Wien-New York, 1984.

W.K.K. Weiwad, W.A. Linke, and M.H.P. Wussling. Sarcomere length-tension relationship of rat cardiac myocytes at lengths greater than optimum. *Journal of Molecular and Cellular Cardiology*, 32:247–259, 2000.

F.E. Zajac. Muscle and tendon: Properties, models, scaling, and application to biomechanics and motor control. *Critical Reviews in Biomedical Engineering*, 17:359–411, 1989.

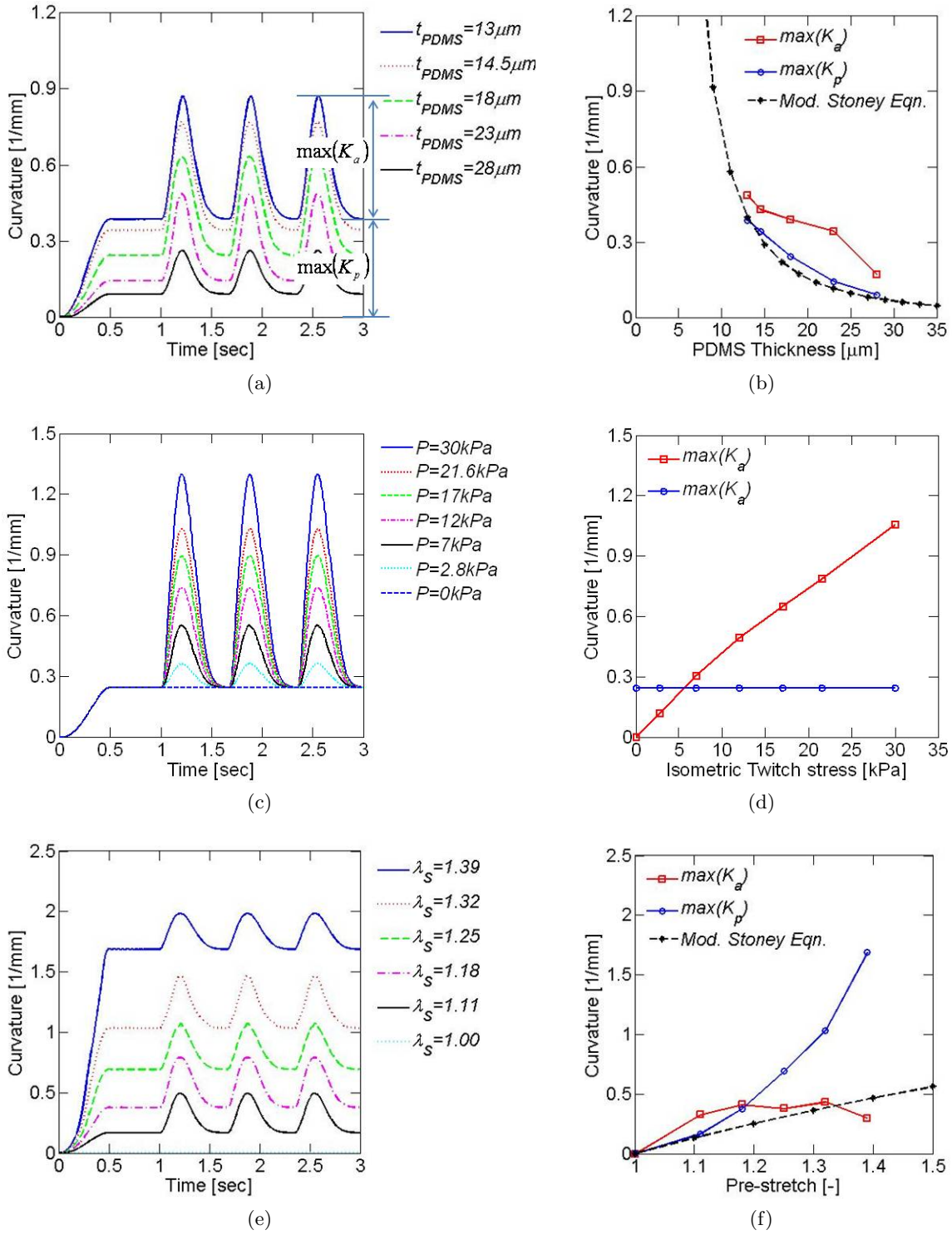

Figure S1: The left column reports the time-curvature plots from FE analysis while the right column the stress contribution of pre-stretch and active response ($max(S_p)$ and $max(S_a)$). (a, b) effect of PDMS thickness, (c, d) Effect of isometric twitch stress of cells, (e, f) effect of cell pre-stretch.